AIChE

Laser Heating of Moving Solid: Influence of Workpiece Speed on Melt Size

Shahzade Z. Shuja, Bekir S. Yilbas, and Omeir Momin
King Fahd University of Petroleum & Minerals, ME Dept., Dhahran 31261, Saudi Arabia

DOI 10.1002/aic.12186
Published online April 20, 2010 in Wiley Online Library (wileyonlinelibrary.com).

Laser heating of a moving solid is considered and phase change in the irradiated region is modeled. Three-dimensional heating situation is considered in the analysis and phase change is modeled using the enthalpy-porosity technique. Temperature field and melt zone are predicted for different workpiece velocities. The predictions are compared with the experimental results. It is found that the maximum temperature in the irradiated region and the size of heat affected zone increase significantly at low workpiece speeds. The prediction of melt depth agrees well with the experimental results. © 2010 American Institute of Chemical Engineers *AIChE J,* 56: 2997–3004, 2010
Keywords: laser, melting, three-dimensional heating, moving work piece

Introduction

High intensity laser heating of surfaces results in phase change in the irradiated region. In most of the industrial applications, laser beam scans the surface with a constant velocity and the solid heating and phase change in the irradiated region extends along the direction of the laser movement. The progressing of the phase change over the workpiece thickness results in cutting or welding of the workpiece. However, the laser surface treatment process requires controlled melting in the surface vicinity. In this case, the process parameters during the laser heating should be selected properly in order to avoid poor quality of the treated surface, such as partial evaporation, and the excessive cost. Moreover, modeling of laser heating process including the phase change provides information on the physical processes taking place during the heating, which can be utilized for the process optimization. Consequently, investigation into laser heating of solid surfaces including the laser scanning speed and phase change in the irradiated material becomes essential.

Correspondence concerning this article should be addressed to B. S. Yilbas at bsyilbas@kfupm.edu.sa.

Considerable research studies are carried out to examine the laser heating of solids and the phase change process. Thermal protection from intense and localized moving heat fluxes using the phase change materials was studied by Cao and Faghri.[1] They used the enthalpy transforming method to formulate the phase change process. Heat conduction in a solid heated by a laser beam was investigated by Modest and Abaicans.[2] They developed the semiclosed form solution for the temperature distribution in the laser heated semi-infinite solid. The numerical modeling of the phase change process using a tracking method was introduced by Vollar and Cross.[3] They used an enthalpy method to approximate the phase change boundary during the heating process. Laser induced vaporization and melting in relation to drilling was investigated by Zhang and Faghri.[4] They obtained the location of solid–liquid and liquid–vapor interface through solving energy conservation equations at the interfaces. Modeling of melt geometry in relation to laser processing was carried out by Tami et al.[5] They used mass and energy balance equations to predict the molten layer during the heating process. The review on high power laser surface treatment of metallic substrates was carried out by Naeem and Saborikanth.[6] They introduced and discussed the laser surface engineering applications for transformation hardening, cladding and alloying. Laser alloying and phase change process was examined by Sarkar et al.[7]

They modeled the phase change process using a fixed-grid enthalpy-porosity technique. The effect of laser beam geometry on the laser transformation hardening was examined by Safdar and Sheikh.[8] They introduced finite element analysis to predict the influence of the spatial distribution of laser power intensity on the temperature field for improved transformation hardening. The model study on transport phenomena in laser surface alloying with distributed species mass source was carried out by Raj et al.[9] The species source term was estimated using the particle-tracking algorithm and a simultaneous particle-melting consideration. The solid–liquid phase change during laser heating process was examined by Krishnan et al.[10] They used the volume-averaged mass and momentum equations with the Brinkman-Forchheimer extension of Darcy's law to model the porous resistance and the enthalpy method was employed to account for the phase change. Laser heating and phase change process was examined by Yilbas and Bin Mansoor[11] and Yilbas et al.[12] They used a two-dimensional heating model, since the heated surface and laser beam were stationary. Moreover, Shuja et al.[13] modeled two-dimensional laser heating process and phase change in the irradiated region. The phase change was modeled using the enthalpy-porosity model. However, the study was limited with two-dimensional heating consideration and three-dimensional effect was left obscure. On the other hand, three-dimensional modeling of laser heating of solid substrate was carried out by Shuja et al.[14,15] However, the studies were limited with the conduction heating only and phase change in the irradiated region was omitted.

In the present study, laser heating of a moving steel and phase change in the irradiated region was considered. The phase change process was modeled using the enthalpy porosity method. To investigate the effect of substrate velocity on the size of the melt and mushy zones, the simulations are repeated for different solid substrate velocities. In the simulations, convective boundary condition is adopted to account for the convective cooling of the irradiated surface by an assisting gas.

Mathematical Modeling of Heating and Phase Change

The heat transfer equation in relation to the laser heating process can be written as[16]:

$$\rho \frac{DE}{Dt} = (\nabla(k\nabla T)) + S_o \tag{1}$$

where E is the energy gain by the substrate material, k is the thermal conductivity, and S_o is the volumetric heat source term and it is:

$$S_o = I_o \delta (1 - r_f) e^{-\delta z} e^{\left(-\frac{x^2+y^2}{a^2}\right)}$$

I_o is laser peak intensity, δ is the absorption depth, a is the Gaussian parameter, r_f is the surface reflectivity, ρ is the density, and x and y are the axes while the laser beam scans the surface along the x-axis. The laser beam axis is the z-axis (Figure 1).

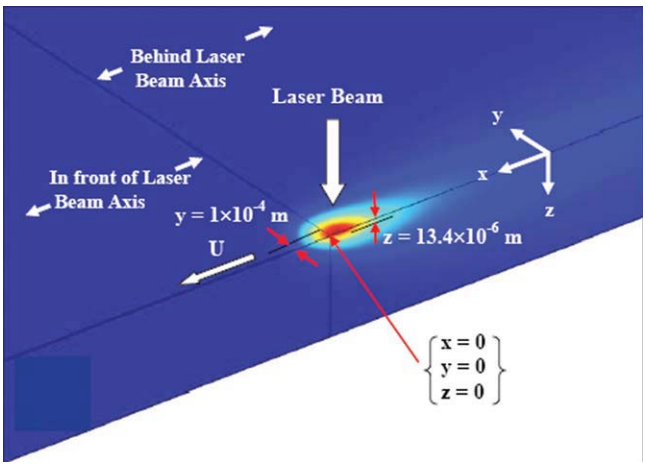

Figure 1. A schematic view of laser heating, workpiece movement, and the coordinate system.

[Color figure can be viewed in the online issue, which is available at wileyonlinelibrary.com.]

In the case of a moving heat source along the x-axis with a constant velocity U, energy gain by the substrate material yields:

$$\rho \frac{DE}{Dt} = \rho \frac{\partial E}{\partial t} - \rho U \frac{\partial E}{\partial x} \tag{2}$$

or

$$\rho \frac{DE}{Dt} = \rho \frac{\partial (CpT)}{\partial t} - \rho U \frac{\partial (CpT)}{\partial x} \tag{3}$$

Combining Eqs. (1) and (3) yields:

$$\rho \frac{\partial (CpT)}{\partial t} = (\nabla(k\nabla T)) + \rho U \frac{\partial (CpT)}{\partial x} + S_o \tag{4}$$

Since the laser scanning speed remains constant, the heating situation can be considered as a steady; in which case the term $\rho \frac{\partial (CpT)}{\partial t}$ in Eq. (4) reduces to zero ($\rho \frac{\partial (CpT)}{\partial t} = 0$).

Equation (4) is solved numerically with the appropriate boundary conditions to predict the temperature field in the substrate material. However, to analyze the phase change problem, the enthalpy-porosity technique is used. In this case, the melt interface is tracked explicitly after defining a quantity called the liquid fraction, which indicates the fraction of the cell volume that is in liquid form. Based on the enthalpy balance, the liquid fraction is computed. The mushy zone is a region in which the liquid fraction lies between 0 and 1. The mushy zone is modeled as a "pseudo" porous medium in which the porosity decreases from 1 to 0 as the material solidifies. When the material has fully solidified in a cell, the porosity becomes zero and hence the velocities also drop to zero.[17]

The enthalpy of the material is computed as the sum of the sensible enthalpy, h, and the latent heat, ΔH:

$$H = h + \Delta H \tag{5}$$

where

Table 1. Material Properties Used in the Simulations (Ref. 21)

	Temp (K)						
Steel	300	400	600	800	1000	1200	1500
C_p (J/kgK)	477	515	557	582	611	640	682
K (W/mK)	14.9	16.6	19.8	22.6	25.4	28	31.7
ρ (kg/m^3)	8018	7968	7868	7769	7668	7568	7418

$$h = h_{ref} + \int_{T_{ref}}^{T} c_p dT \tag{6}$$

and

h_{ref} = reference enthalpy
T_{ref} = reference temperature
c_p = specific heat at constant pressure
The liquid fraction, β, can be defined as:
$\beta = 0$ if $T < T_{solidus}$
$\beta = 1$ if $T > T_{liquidus}$

$$\beta = \frac{T - T_{solidus}}{T_{liquidus} - T_{solidus}} \quad \text{if} \quad T_{solidus} < T < T_{liquidus} \tag{7}$$

Equation 7 is referred to as the lever rule.[17]

The latent heat content can now be written in terms of the latent heat of the material, L:

$$\Delta H = \beta L \tag{8}$$

The latent heat content can vary between zero (for a solid) and L (for a liquid).

The solution for temperature is essentially iteration between the energy equation [Eq. (4)] and the liquid fraction equation [Eq. (7)]. Directly using Eq. (7) to update the liquid fraction usually results in poor convergence of the energy equation. However, the method suggested by Voller and Prakash[18] is used to update the liquid fraction based on the specific heat.

To solve Eq. (4), two boundary conditions for each principal axis should be specified. Because of the assisting gas, the convective boundary is assumed at the surface, and at a distance considerably away from the surface (at infinity). As the depth of liquid region is significantly less than the thickness of the workpiece, the problem can be considered as the semi infinite-body and this assumption simplifies the solution of the problem. The boundary conditions, therefore, are:

z at infinity $\Rightarrow\ z = \infty : T(r, \infty, t) = T_o$ (specified)
r at infinity $\Rightarrow\ r = \infty : T(\infty, z, t) = T_o$ (specified)
At symmetry axis $\Rightarrow\ r = 0 : \dfrac{\partial T(0, z, t)}{\partial r} = 0$
At the surface $\Rightarrow\ z = 0 : k\dfrac{\partial T(r, 0, t)}{\partial z} = h_t(T_s - T_\infty)$

where h is the heat transfer coefficient t at the free surface. The heat transfer coefficient predicted earlier[19] is used in the present simulations ($h_t = 10^4$ W/m^{2}K). However, it is observed from the simulations that some small changes in the heat transfer coefficient ($\pm 10\%$) does not affect temperature field.

Numerical Solution

To discretize the governing equation [Eq. (4)], a control volume approach is introduced. The details of the numerical scheme are given in Ref. 20. The calculation domain is divided into grids and a grid independence test is performed for different grid sizes and orientation. A nonuniform grid with $90 \times 45 \times 55$ mesh points along x, y, and z axes, respectively, is employed after securing the grid independence. The finer grids are located near the irradiated spot center in the vicinity of the surface and grids become courser as the distance increases towards the bulk of substrate material. The central difference scheme is adopted for the diffusion terms. The convergence criterion for the residuals is set as $|\psi^k - \psi^{k-1}| \leq 10^{-6}$ to terminate the simulations. Table 1 gives the thermal properties of material used in the simulations. The laser power is kept the same as the experimental value in the simulations, i.e., Gaussian parameter $a = 2/3 \times R$ (R is a laser beam radius at the workpiece surface $R = 0.3$ mm) and power intensity $I_o = 0.8 \times 10^9$ W/m^2.

The Fluent software is used in the simulations to predict temperature field in the heated workpiece. Moreover, the user defined functions are introduced in the Fluent code to account for the laser heating source and the convective boundary condition.

Experimental

The laser used in the experiment is a CO_2 laser (LC-αIII-Amada, Amada BP 41040, 95912 Roissy Aeroport Cedex, France) and delivering nominal output power of 2000 W with adjustable duty cycle. Nitrogen emerging from a conical nozzle and coaxially with the laser beam is used. 127-mm focal lens is used to focus the laser beam, which results in the focal radius of 0.3 mm at the surface. The laser heating parameters are given in Table 2.

Scanning electron microscopy is carried out to obtain the micrographs of the laser irradiated cross-section.

Table 2. Laser Heating Parameters

Duty Cycle	Power (W)	Nozzle Gap (mm)	Nozzle Diameter (mm)	Focus Diameter (mm)	N_2 Pressure (kPa)	a (m)
0.4	230	1.5	1.5	0.8	400	0.2×10^{-3}

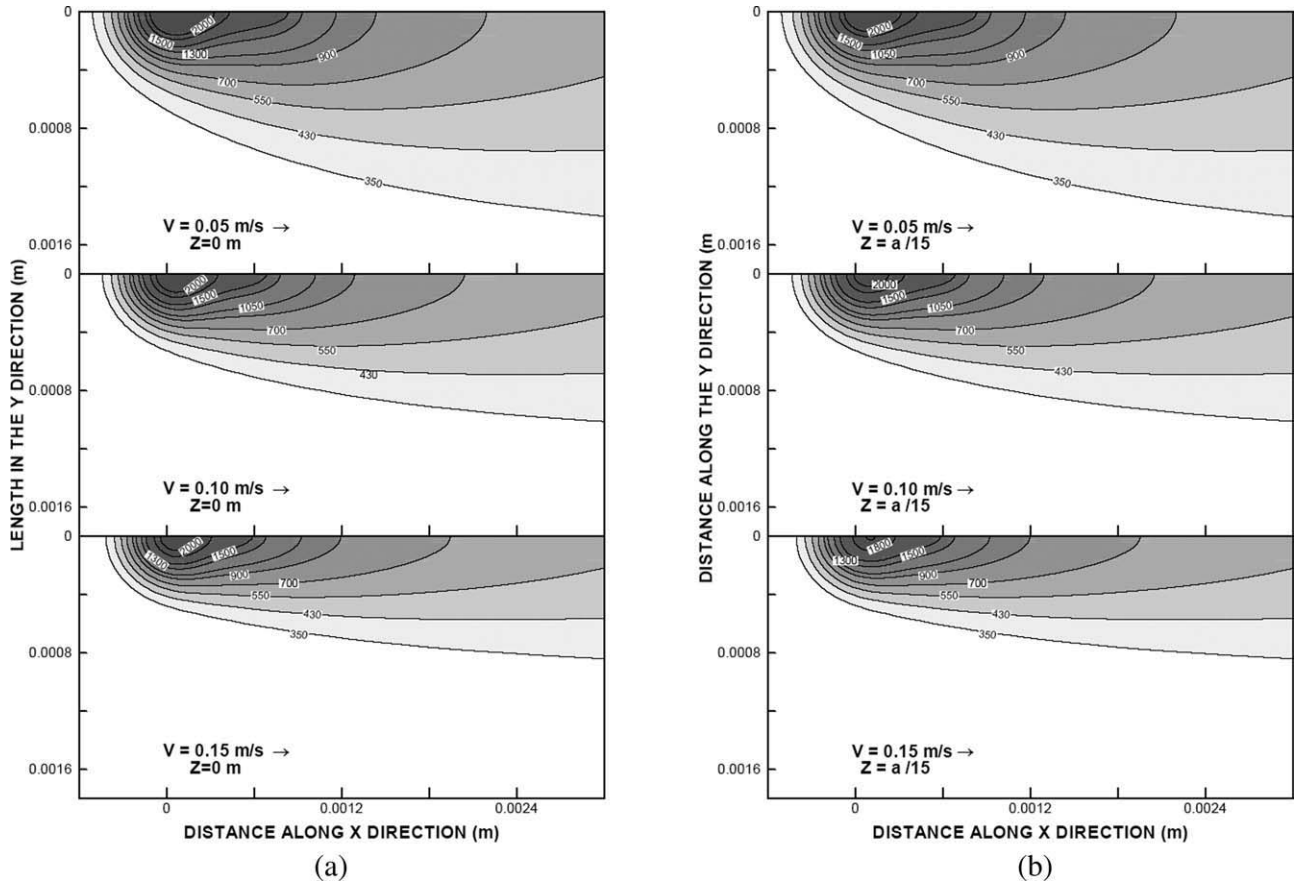

Figure 2. (a) Temperature contours in *x*, *y* plane, and $z = 0$ m for different workpiece speeds. (b) Temperature contours in *x*, *y* plane, and $z = 13.4 \times 10^{-6}$ m below the surface for different workpiece speeds.

Results and Discussion

Laser heating of a moving steel workpiece is considered and the phase change in the irradiated region is modeled. The influence of the workpiece speed on the temperature field and the melt depth is examined. The convective boundary at the free surface of the workpiece is considered to resemble the assisting gas during the heating process.

Figures 2a,b show temperature contours in the x, y plane at $z = 0$ (at the free surface of the work piece) and $z = 13.4 \times 10^{-6}$ m (below the surface) for three different workpiece speeds. Temperature attains high values in the region close to the laser beam axis and as the distance increases away from the irradiated spot center, it reduces particularly in the region in front of the laser beam as reference to the workpiece movement. Temperature contours extend towards the rear side of the beam because of the initial heating of the workpiece by a laser beam during the workpiece movement. The development of high temperature ($T > 1500$) in the irradiated region is the indication of the melting. The laser power intensity is set accordingly to avoid the evaporation of the surface. This is necessary for the practical laser heating applications to prevent the high surface roughness in the heated region, since surface evaporation results in undulation and irregular cavity formation at the surface.[22] The influence of workpiece speed on temperature distribution is considerable, particularly along the y-axis. In this case, temperature contours extend along the y-axis at low workpiece speed. This is because of the rate of heat transfer from the laser heating source to the workpiece, which remains high for low workpiece speeds. Moreover, this argument is true for Figure 2b, provided that the size of heated region reduces, since the size of extension of isothermals is not as wide as those corresponding to the free surface ($z = 0$ m). The influence of convective cooling at the surface is not significant, since temperature remains high in the surface region as compared to some depth below the surface. This is because of the heat transfer coefficient, which is selected as $h_t = 10^4$ W/m^{2}K in line with the previous work.[19] It should be noted that the heat transfer coefficient less than 10^7 W/m^{2}K does not have notable effect on temperature rise in the surface region during the laser heating process.[23]

Figure 3 shows contour plots of temperature in the x-z plane, where y-axis location is $y = 0$ m for three workpiece speeds. Temperature contours extends further into the substrate material for low workpiece speeds. However, the extension of temperature contours along the y-axis is not as large as its counterpart corresponding to the z-axis. This is because of the temperature gradient, which is significantly higher along the z-axis than that of y-axis. The high temperature gradient results in high rate of heat transfer for surface

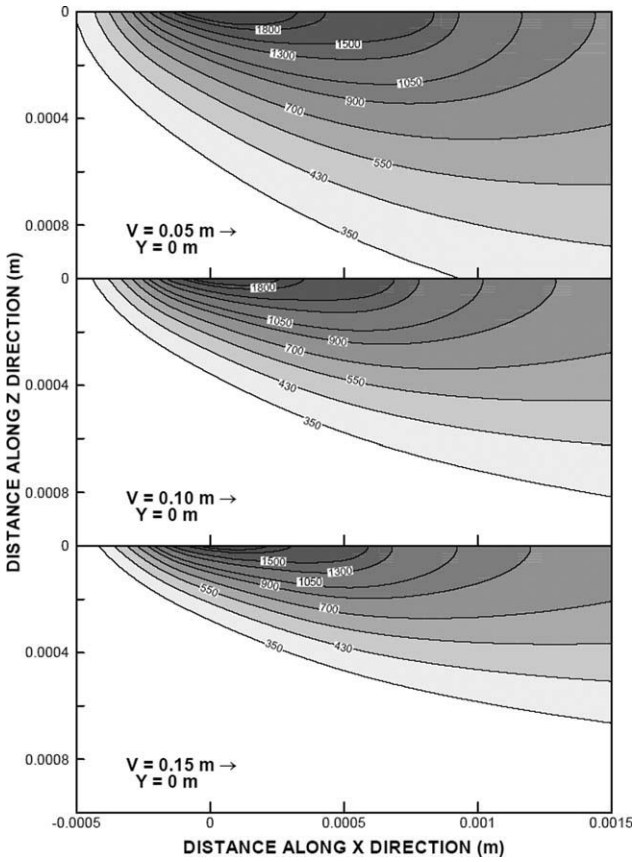

Figure 3. Temperature contours in *x*, *z* plane, and *y* = 0 m for different workpiece speeds.

region to solid bulk. In addition, the Gaussian distribution of the laser power intensity at the surface results in the maximum intensity in the region of the irradiated spot center and it reduces as the distance along the *y*-axis increases away from the irradiated spot center. This contributes to the attainment of high temperature gradient along the *z*-axis. It should be noted that the location of the maximum temperature moves slightly away from the irradiated spot center due to the movement of the workpiece. It is also evident that the depth of melt region where temperature above 1600 K extends almost 90 μm below the surface for a workpiece speed of 0.05 m/s. However, as the workpiece speed increases the depth of melt layer reduces significantly, i.e., it becomes almost 15 μm for 0.15 m/s workpiece speed. In addition, the heat affected zone reduces to almost half as the workpiece speed increases to 0.15 m/s. Consequently, the workpiece speed has significant effect on the size of the melt and heat affected zones.

Figure 4 shows surface temperature profiles along the *x*-axis for three *y*-axis locations (see Figure 1) and three workpiece speeds. It should be noted that the temperature attains the maximum at a location slightly away from the irradiated spot center. The distance along the *x*-axis $x < 0$ m represents the region in front of the laser spot center while $x > 0$ m is the distance behind the heated spot center as reference to the workpiece movement. Temperature decays sharply in the region in front of the irradiated spot. However, temperature decays gradually in the region behind the irradiated spot. Moreover, the temperature gradient is very large in front of the irradiated spot so that the phase change is not observable. On the other hand, superheating of liquid phase and melt initiation at constant temperature is evident in the region behind the irradiated spot center. This is particularly true for $y = 0$ m. Moreover, reducing workpiece speed increases the temperature at the surface, which is true for all the *y*-axis locations. The superheating of liquid phase dominates over the conduction heating in the irradiated region at the workpiece surface at low workpiece speed. Consequently, the magnitude of the maximum temperature at the surface can be altered while controlling the workpiece speed. Temperature gradient in the solid region next to the melted zone is higher for all the speeds. However, as the distance along the *x*-axis increases away from the melt edge, the temperature gradient becomes small. This indicates that the heat conduction in the region next to the edge of the melt zone is significantly higher as compared to the region away from the melt zone edge. This high rate of conducted energy suppresses the size of the melt zone at the irradiated surface. Consequently, at distances $y = a/2$ and $y = 3a/2$ (a is the Gaussian parameter and $a = 0.2$ mm), the constant temperature line is not clearly observable from the figures, except at the low workpiece speed. It should be noted that the laser pulse intensity distribution along the *y*-axis contributes to the

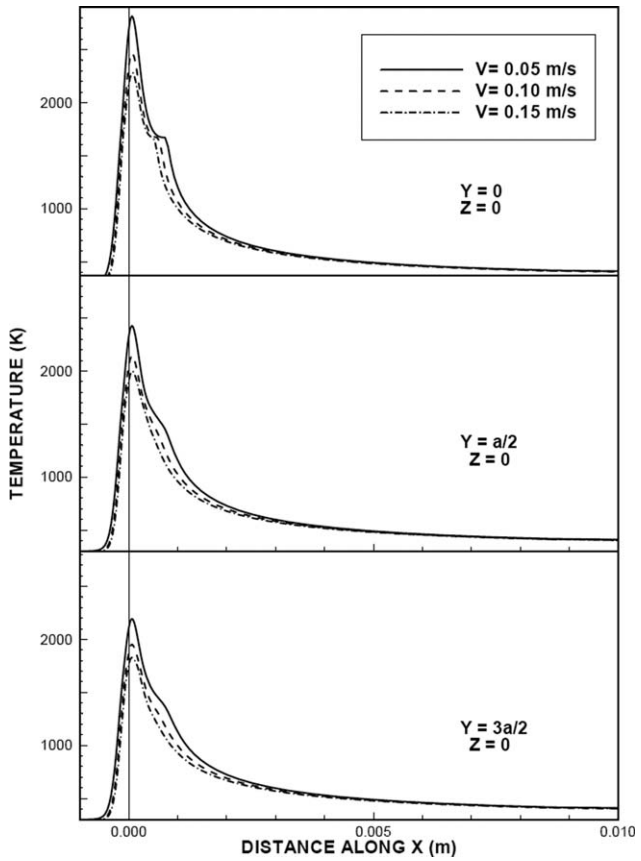

Figure 4. Temperature distributions along the *x*-axis at different *y*-axis locations for different workpiece speeds.

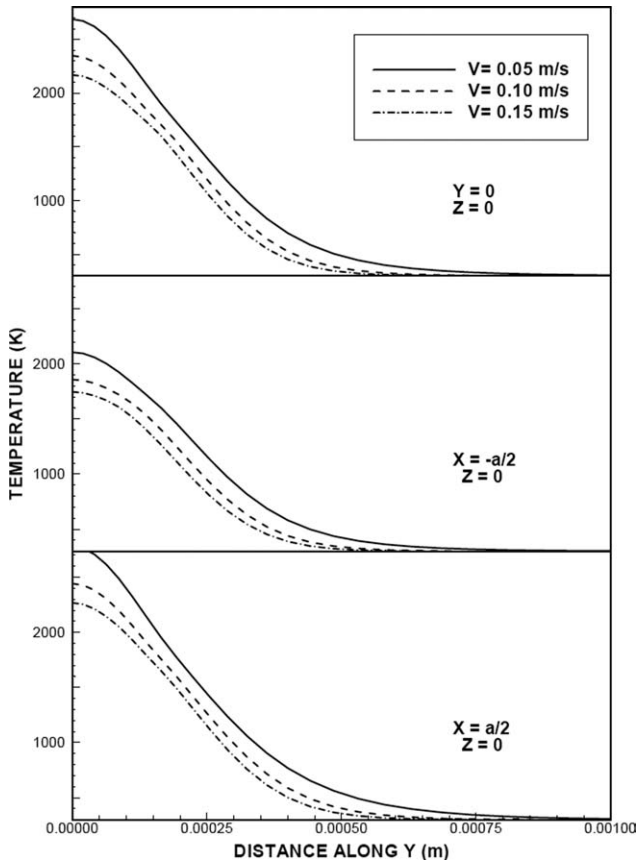

Figure 5. Temperature distributions along the *y*-axis at different *x*-axis locations for different workpiece speeds.

attainment of small melt zone along the y-axis at the surface, since the laser power intensity decays exponentially along the y-axis (Gaussian intensity profile).

Figure 5 shows temperature distribution along the y-axis for different x-axis locations and for three workpiece speeds. It should be noted that $x = -a/2$ is the x-axis location in front of the irradiated spot center, $x = 0$ is the x-axis location of the irradiated spot center, and $x = a/2$ is the location behind the irradiated spot center along the x-axis as reference to the workpiece movement (Figure 1). Temperature decays gradually in the irradiated region $y \leq 0.1$ mm. As the distance from the edge of the irradiated region extends away from the edge, temperature decays sharply while resulting in large temperature gradient in this region. The gradual decrease of temperature gradient along the y-axis is associated with the laser power intensity distribution and the heat transfer along the y-axis. In this case, the Gauss distribution of the laser power intensity modifies the heat transfer rate along the y-axis and super heating of liquid along the y-axis suppresses the change in temperature distribution. Although temperature profile, in general, is not influenced by the workpiece speed, the value of the maximum temperature reduces at $y = 0$ with increasing workpiece speed. This is true for all the x-axis locations selected at the workpiece surface.

Figure 6 shows temperature distribution along the z-axis at different x-axis locations for three different workpiece speeds. Temperature decay is sharp in the region next to the surface and as the distance increases towards the solid bulk, temperature decay becomes gradual. This is true for all workpiece speeds and x-axis locations. Temperature attains the maximum at the surface and the depth of liquid zone ($T \geq 1600$ K) extends about 90 μm below the surface for the location $x = 0$. However, the depth of liquid layer changes at different x-axis locations as well as with the workpiece speed. As the decay of temperature is sharp in the surface region, the melting initiation at constant temperature is not clearly notable from the curves. This is true for all workpiece speeds. However, slight changes in temperature profile are observed around the melting temperature for a workpiece speed of 0.15 m/s. The sharp decay of temperature below the surface enhances the heat conduction from the surface region to the solid bulk. This results in extension of heat effected zone below the surface, which is more pronounced for the workpiece speed of 0.05 m/s. Therefore, reducing the workpiece speed enhances the depth of liquid layer and the depth of the heat effected zone within the irradiated region inside the workpiece.

Figure 7 shows SEM micrograph of close view of laser melted zone. It is evident from SEM micrograph that the melt layer extended almost 95 μm below the surface and demarcation line at the melt boundary is also evident. When comparing the experimental data and the predictions, it can

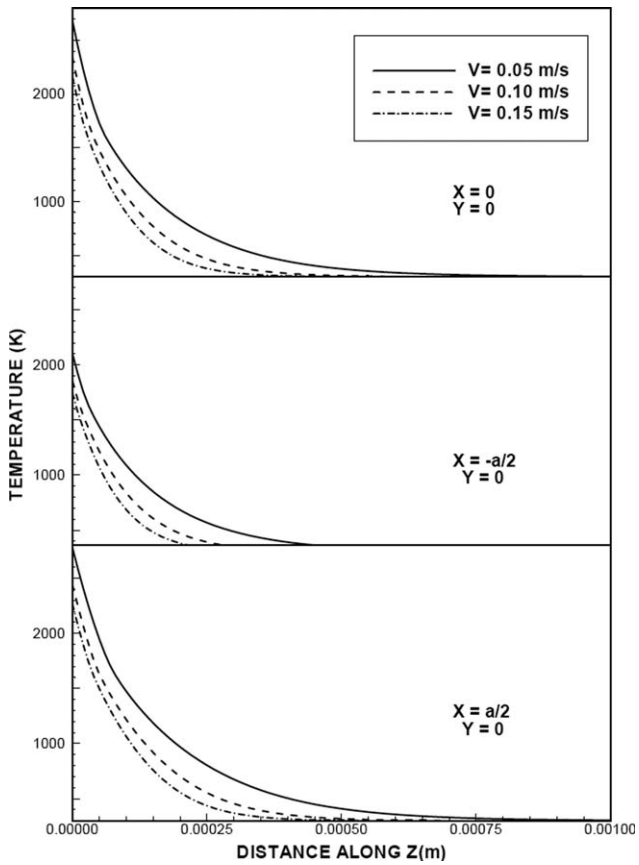

Figure 6. Temperature distributions along the *z*-axis at different *x*-axis locations for different workpiece speeds.

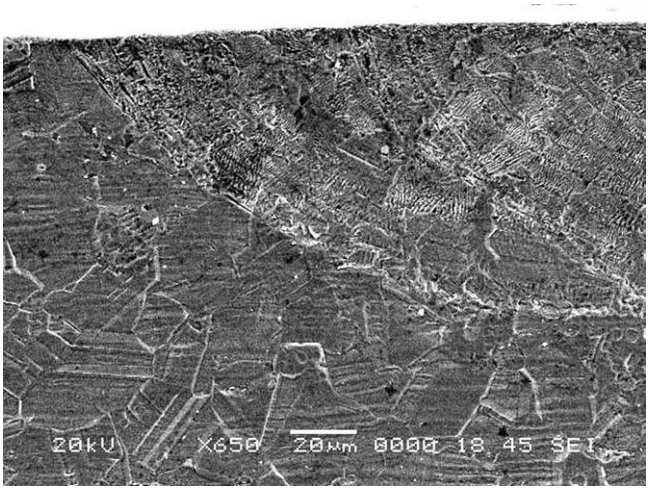

Figure 7. SEM micrographs of cross-section of laser melted region. Laser scanning speed is V = 0.05 m/s.

be seen that both results are in agreement, i.e., the melt depth predicted is in the order of 100 μm. However, discrepancies between the two results are due to one or all of the following reasons; (i) the assumptions made in the simulation such as uniform properties and (ii) experimental errors, which are estimated as 6%. Nevertheless, the difference between the two results is negligible.

Conclusions

Laser heating of moving steel is considered and phase change in the irradiated region is modeled. In the analysis, three-dimensional model is incorporated and the enthalpy porosity technique is used to account for the phase change in the irradiated region. It is found that the temperature decays sharply in the region in front of the irradiated spot center as reference to the workpiece movement while the decay is gradual behind the irradiated spot center. The gradual decay of temperature is associated with the initial heating of the workpiece due to its motion. The super heating of liquid phase occurs in the irradiated region and temperature decay is sharp in the region next to the liquid phase boundary. However, as the distance increases from the liquid boundary, temperature decay becomes gradual. The sharp decay in temperature results in high rate of heat flux from high temperature region to low temperature region. This, in turn, suppresses the enlargement of melt zone while increasing the size of heat affected zone. This situation is observed at low workpiece speed; in which case temperature attains the maximum at the irradiated zone as compared to its counterparts corresponding to the high scanning speeds. The depth of the melt zone extends almost 90 μm below the surface for workpiece speed of 0.05 m/s. However, increasing workpiece speed lowers the depth of the melt zone. The results predicted for the melt depth agrees well with experimental results, provided that some discrepancies between both results are because of the assumptions made in the model study, such as uniform thermal properties, and the experimental error, which is the order of 6%.

Acknowledgments

The authors acknowledge the support of King Fahd University of Petroleum and Minerals, Dhahran Saudi Arabia.

Notation

a = Gaussian parameter (m)
A_{mush} = mushy zone constant
c_{p} = specific heat capacity $\left(\frac{\text{J}}{\text{kgK}}\right)$
H = total enthalpy $\left(\frac{\text{J}}{\text{k}}\right)$
h = enthalpy $\left(\frac{\text{J}}{\text{kgK}}\right)$
h_{ref} = reference enthalpy $\left(\frac{\text{J}}{\text{kgK}}\right)$
h_{t} = heat transfer coefficient $\left(\frac{\text{W}}{\text{m}^2\text{K}}\right)$
I_{o} = laser peak power intensity $\left(\frac{\text{W}}{\text{m}^2}\right)$
k = thermal conductivity $\left(\frac{\text{W}}{\text{mK}}\right)$
T = temperature (°C)
T_{liquidus} = liquid temperature (°C)
T_{solidus} = solid temperature (°C)
t_{c} = end of cooling period (s)
t_{f} = beginning of falling period of the consecutive pulse(s)
t_{p} = pulse length of the consecutive pulse (s)
t_{r} = end of rise period of the consecutive pulse (s)
r = radial distance (m)
r_{f} = reflection coefficient
S = momentum sink per unit mass flow rate$\left(\frac{\text{m}}{\text{s}}\right)$
S_{o} = source term (W/m^3)
T_{o} = initial temperature (°C)
t = time (s)
z = axial distance (m)

Greek letters

β = The liquid fraction
ε = porosity
ρ = density $\left(\frac{\text{kg}}{\text{m}^3}\right)$
$\alpha(=\frac{k}{\rho Cp_{\text{s}}})$ = thermal diffusivity $\left(\frac{\text{m}^2}{\text{s}}\right)$
δ = absorption depth (m^{-1})

Literature Cited

1. Cao Y, Faghri A. Thermal protection from intense localized moving heat fluxes using phase-change materials. *Int J Heat Mass Transfer*. 1990;33:127–138.
2. Modest MF, Abakians H. Heat conduction in a moving semi-infinite solid subjected to pulsed laser irradiation. *J Heat Transfer*. 1986; 108:597–601.
3. Voller V, Cross M. An explicit numerical method to track a moving phase change front. *Int J Heat Mass Transfer*. 26; 1983:147–150.
4. Zhang Y, Faghri A. Vaporization, melting and heat conduction in the laser drilling process. *Int J Heat Mass Transfer*. 1999;42:1775–1790.
5. Tani G, Tomesani L, Campana G. Prediction of melt geometry in laser cutting. *Appl Surf Sci*. 2003;208/209:142–147.
6. Naeem M, Sabarikanth R.*High power CW Nd:YAG laser beam surface modification*. In: Sudarshan TS, Sundararajan G, Totten GE, Joshi SV (Eds). *Proceedings of the International Conference on Advances in Surface Treatment: Reaearch and Applications, ASTRA*. ARCI, Hyderabad, India. Society for Advancement of Heat Treatment & Surface Engineering (SAHTSE) 2004:224–228.
7. Sarkar S, Raj PM, Chakraborty S, Dutta P. Three-dimensional computational modeling of momentum, heat and mass transfer in a laser surface alloying process, *Numer Heat Transfer A*. 2002;42:307–326.
8. Safdar S, Li L, Sheikh MA. Numerical analysis of the effects of non-conventional laser beam geometries during laser melting of metallic materials. *J Phys D: Appl Phys*. 2007;40:593–603.
9. Raj PM, Sarkar S, Chakraborty S, Phanikumar G, Dutta P, Chattopadhyay K. Modelling of transport phenomena in laser surface alloying with distributed species mass source. *Int J Heat Fluid Flow*. 2002;23:298–307.
10. Krishnan S, Murthy JY, Garimella SV. Analysis of solid-liquid phase change under pulsed heating. *J Heat Transfer*. 2007;129:395–399.

11. Yilbas BS, Mansour SB. Laser evaporative heating of surface: simulation of flow field in the laser produced cavity. *J Phys D: Appl Phys*. 2006;39:3863–3875.
12. Saad BM, Yilbas BS, Shuja SZ. Laser pulse heating: modeling of cavity formation. *Proc Inst Mech Eng C: J Mech Eng Sci*. 2007;221:307–328.
13. Shuja SZ, Yilbas BS, Khan S. Laser consecutive pulse heating in relation to melting influence of duty on melting. *Heat Mass Transfer*. 2009;45:793–803.
14. Shuja SZ, Yilbas BS, Budair MO. Modeling of laser heating of solid substance including assisting gas impingement. *Numer Heat Transfer A*. 1998;33:315–339.
15. Shuja SZ, Yilbas BS, Khan S. Laser consecutive pulse heating and phase change: influence of spatial distribution of laser pulse intensity on melting. *Int J Therm Sci*. 2009;48:1960–1966.
16. Yilbas BS, Arif AFM, Abdul Aleem BJ. Laser cutting of holes in thick metals: development of stress field. *Opt Lasers Eng*. 2009;47:909–916.
17. Fluent Inc. *Fluent Users Guide*. Florida, USA: Fluent Inc. 2005.
18. Voller VR, Prakash C. A fixed-grid numerical modeling methodology for convection-diffusion mushy region phase-change problems. *Int J Heat Mass Transfer*. 1987;30:1709–1720.
19. Shuja SZ, Yilbas BS. Pulsative heating of surfaces. *Int J Heat Mass Transfer*. 1998;4:3899–3918.
20. Patankar SV. *Numerical Heat Transfer*, 1st ed. New York: McGraw-Hill, 1980.
21. Incropera FP, DeWitt DP. *Fundamentals of Heat and Mass Transfer*, 4th ed. New York: John Wiley, 1996:829–830.
22. Yilbas BS, Shuja SZ. Laser treatment and PVD coating of Ti-6Al-4V alloy. *Surf Coat Technol*. 2000;130:152–157.
23. Yilbas BS, Shuja SZ, Budair MO. Nano-second pulse heating and gas assisting jet considerations, *Int J Machine Tools Manuf*. 2000; 40:1023–1038.

Manuscript received Nov. 1, 2009, and revision received Jan. 1, 2010.